Smart Pipeline Structural Health Monitoring of Crack or Fracture Propagation using Piezoelectric Sensors

Wadie Chalgham[*1], Gregory Carman[1], Ali Mosleh[1]
1. Mechanical and Aerospace Engineering Department, University of California, Los Angeles (UCLA), Los Angeles, CA, USA
* Contact author: wadie.chalgham@ucla.edu

Abstract: This paper proposes a solution method using piezoelectric sensors to detect an anomaly, such as a deformation caused by a crack or fracture, in a pipeline. COMSOL Multiphysics, a simulation software, is used to induce anomalies of different magnitudes to a pipe and record the data from the piezoelectric sensor, which is placed along the pipeline. The anomalies are in a form of deformations caused by changing the voltage across the piezoelectric material. Analysis of the simulation results showed a relationship between the magnitude of the deformation of the pipe in the xy, xz, and yz directions and the magnitude of the voltage across the piezoelectric patch. In addition, the paper studied the behavior of the deformation with respect to time by including time-dependent relationships in the propagation of voltage through the piezoelectric patch along the pipe surface. Pipeline integrity supervisors can use the equations presented in this paper which relate the voltage read across the piezoelectric sensor, the deformation of the pipe, and the velocity of the crack propagation as baseline data to detect the existence of an anomaly. Finally, the simulation results from this paper can be used to detect not only the existence of an anomaly but also its type (crack, fracture, leak, or corrosion) as well as its location with high accuracy based on machine learning algorithms or advanced statistical analysis methods.

Keywords: Structural Health Monitoring, Piezoelectric Sensor, Numerical Simulation

Introduction

Structural Health Monitoring for Pipelines needs solutions that have low installation and maintenance costs, consume minimal power, measure and send data continuously and wirelessly, operate easily, and detect the anomalies as well as their types and location with high accuracy. Anomaly detection represents an essential aspect in pipeline rehabilitation to avoid any unexpected failure. Several detection techniques have been adopted and received widespread application in pipeline inspection nowadays, but they still present major challenges to field operators.

Anomaly detection techniques are categorized into two main groups: non-continuous and continuous methods. Non-continuous methods include inspection by helicopter, drones, smart pigging, trained dogs, and mobile untethered tools detecting leaks inside the pipeline [1–6]. Continuous methods could be either external by detecting leaks outside the pipe or internal by using field measurement like pressure or flow variation to monitor internal pipeline conditions. External continuous methods include fiber optic cable, acoustic sensor, video monitoring, and wireless sensor node System on Chip (SoC) [7]. Internal continuous methods, however, include pressure point analysis, mass balance, and statistical system [8]. The performance of all these methods varies and depends on many factors such as hardware quality and sensors accuracy. Moreover, other methods have a high false alarm redundancy (fiber optic cable, acoustic sensor, video monitoring) and almost all of them have very high installation, operation and maintenance cost [9].
Some researchers proposed the concept of using piezoelectric sensors to detect anomalies in pipelines, but they were limited to detecting one type of anomaly only [10-13]. In [10], the main goal was to monitor the structural health of a facility by monitoring the bolts loosening while in [11] the goal was to monitor the bolts loosening using minimal power consumption for the sensors. In [12], the goal was to monitor the health of a pipeline by analyzing the corrosion status, and in [13], the main goal was to detect leaks of gas pipelines. None of the previously described papers presented a technique to find the anomaly type based on the piezoelectric sensor data, which is critical in practice where the type of anomaly is unknown, especially for underground pipelines. Nowadays, not a single system is universally accepted as a preferred method since all have strengths and weaknesses, though some are far more commonly used than others. Moreover, most pipelines are typically inspected at intervals of several years, and all used techniques have some limitations related to detecting in-situ defects. Most of the anomaly detection techniques do not provide fast and real-time monitoring of the entire pipe length and use wired sensors which get damaged easily, and they require periodic maintenance, and have high installation costs [14].

This paper proposes a smart pipeline structural health monitoring method using piezoelectric sensors to detect anomalies in the pipe in the different directions and the rate of propagation of the induced deformation along the pipeline. The proposed method is an economic and effective solution to detect anomalies in real-time. The relationship between the voltage and the deformation magnitude results outlined in this paper can then be used to detect the anomaly type such as a crack, fracture, leak, or corrosion while the relationship between crack propagation rate and deformation magnitude results can be used to detect the location of the anomalies with high accuracy.

Numerical Model

In this section, first the model of a pipeline is built in a modeling finite element software, COMSOL Multiphysics 5.3. Figure 1 shows the overall geometry implemented for the numerical study. It shows that the pipe has a length of 100 mm, an inner radius of 6 mm, and an outer radius of 10 mm, along with a piezoelectric patch with dimensions of 5×2×5 mm for width, depth, and height, respectively. The piezoelectric material is placed in the middle of the pipe at a distance of 50 mm.

The pipe is made out of Aluminum and its material parameters are presented in Table 1 in the Appendix. The piezoelectric patch is made of Lead Zirconate Titanate (PZT-5H), and its material parameters are presented in Table 2 in the Appendix. In addition, the settings used for the Strain-charge form of the PZT patch, and the corresponding setting used for Stress-charge from are presented in Tables 3 and 4 in the Appendix respectively. The fluid flowing through the pipeline is water and its material parameters are presented in Table 5 in the Appendix.

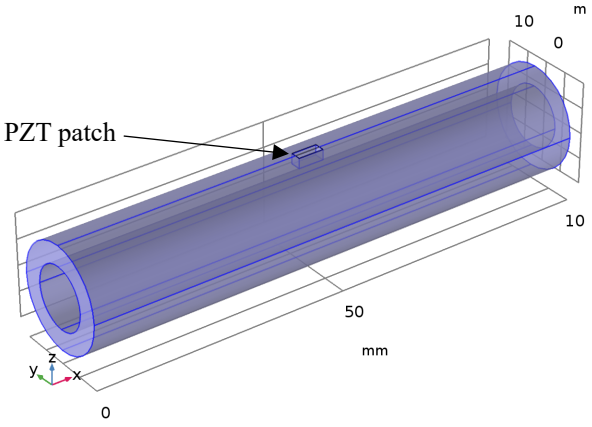

Figure 1. Geometry of the pipeline with the PZT patch

Theory and Governing Equations

In order to simulate the piezoelectric effect, a multi-physics study is conducted to combine solid mechanics and electrostatics. For the solid mechanics study, it is assumed that the pipe is made of linear elastic material which its initial displacement and structural velocity fields are zero. For the piezoelectric material, it is assumed that the temperature is 293.15 K. In addition, it is assumed that the left end of the pipe is a fixed constraint. For the electrostatics study, it is assumed that the edges of the PZT patch have a zero charge, and that the initial charge across the piezoelectric material is zero. In addition, the electric potential is supplied from the lower part of the PZT. The following coupled constitutive equations are assumed before running the simulation of the electrostatics study:

$$T = c_E S - e^T E \quad \text{(Eq. 1)}$$
$$D = eS + \epsilon_S E \quad \text{(Eq. 2)}$$
$$S = s_E T - d^T E \quad \text{(Eq. 3)}$$
$$D = dT + \epsilon_T E \quad \text{(Eq. 4)}$$

where T is the stress in [Pa], S is the strain, E is the electric field in [N/C], and D is the electric displacement in [C/m^2]. Eq.1 and Eq.2 describe the stress-charge relationship while Eq.3 and Eq. 4 describe the strain-charge relationship. Moreover, $\boldsymbol{c_E}$ is the elasticity matrix (rank 4 tensor $\boldsymbol{c_{ijkl}}$) in [Pa] which can be found using Eq.5, **e** is the coupling matrix (rank 3 tensor $\boldsymbol{e_{ijk}}$) in [C/m^2] which can be found using Eq.6, and $\boldsymbol{\epsilon_S}$ is the permittivity matrix (rank 2 tensor $\boldsymbol{\epsilon_{ij}}$) in [C^2 N^{-1} m^{-2}] which can be found using Eq.7.

$$c_E = s_E^{-1} \quad \text{(Eq. 5)}$$
$$e = ds_E^{-1} \quad \text{(Eq. 6)}$$
$$\epsilon_S = \epsilon_T - ds_E^{-1} d^T \quad \text{(Eq. 7)}$$

The next step is to perform two analyses: a stationary study and a time-dependent study. For the stationary study, anomalies are induced in the pipeline by providing a voltage of 20 volts across the PZT patch where the positive end is towards the inner radius of the pipe, and the ground is towards the surface.
For the time-dependent study, the voltage of 20 V is induced with a time step of 2 volts per second. This study aims at analyzing the relationship between the rate of voltage increase across the PZT sensor and the magnitude of the deformations. The expected results are deformations along the pipe in the different directions (xy, xz, and yz) and different deformation

magnitudes for different voltage charges across the PZT patch.
Finally, a mesh convergence study is performed. It is shown that for a given mesh, when the mesh size increases by a factor of 2, the mesh converges. Table 6 in the Appendix presents the mesh properties.

Simulation Results

This section provides the results of the simulations described in the previous sections. The results aim at showing the deformations inside as well as on the surface of the pipeline when an electric potential is applied through the piezoelectric material. The results show also these deformations in the different planes, i.e. xz, xy, and yz. The purpose of the simulation results analysis is to find a correlation between the deformations in the pipe and the electric potential across the PZT patch.

In order to observe the overall effect of the electric potential on the pipe outer surface, surface plots of the pipe are plotted at different electric potentials. Figure 2a shows the initial pipe state with no induced electric charge, and it shows that no deformations are occurring as expected. Figure 2b shows the pipe deformation when 10 volts are applied to the piezoelectric material. It shows that the pipe is deformed towards the surface of the outer radius, creating a gap inside the pipe. At this voltage, a maximum of 3.14 x 10^{-6} mm deformation is observed. Figure 2c shows the pipe deformation when the voltage is double to 20 volts. It shows that the pipe is further deformed towards the surface of the outer radius, creating a bigger gap inside the pipe. At this voltage, the maximum deformation doubled to 6.29 x 10^{-6} mm. Figure 2 shows a linear relationship between the maximum deformation observed at the pipe and the voltage induced through the PZT patch.

In order to understand the deformation propagation across the different planes, slices are created to observe the deformation magnitude in the xz, xy, and yz planes. Figure 3 shows the xz pipe cross section of deformations when 20 volts are induced across the PZT patch. It shows a maximum deformation of 6.29 x 10^{-6} mm as expected, which is similar to the value observed in Figure 2c. In fact, since the electric potential is induced in the xz direction, it makes sense that the maximum deformations across the pipe are along the xz plane too.

In order to observe the increase of the deformation in this plane to the maximum value presented above, a line was created at the top surface of the pipe model along which deformation data was collected as shown in Figure 4. This figure shows a plot of the corresponding results, of the total displacement magnitude in mm versus the pipe x-axis.

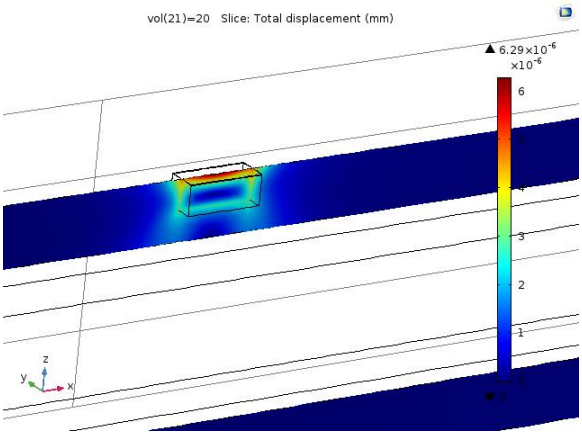

Figure 3. xz pipe cross section of deformations when 20 volts are induced across the PZT patch

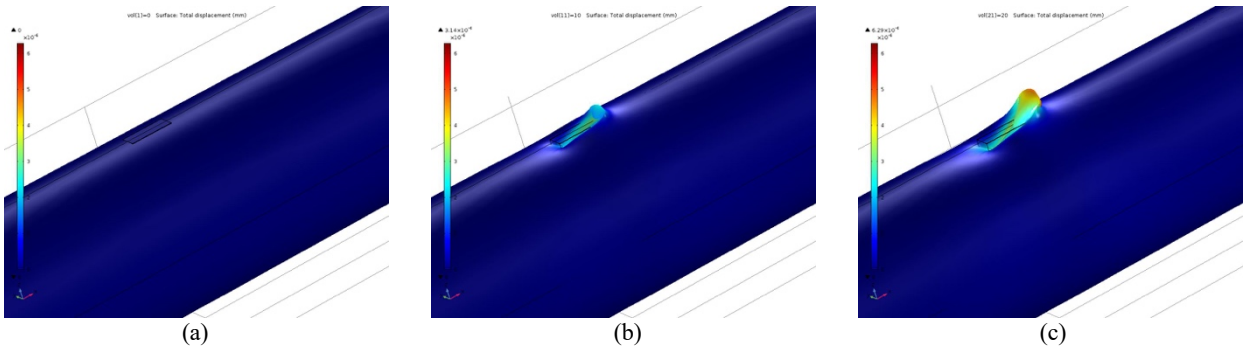

(a) (b) (c)

Figure 2. Pipe deformation when (a) no electric charge induced, (b) 10 volts are induced across the PZT patch, and (c) 20 volts are induced across the PZT patch

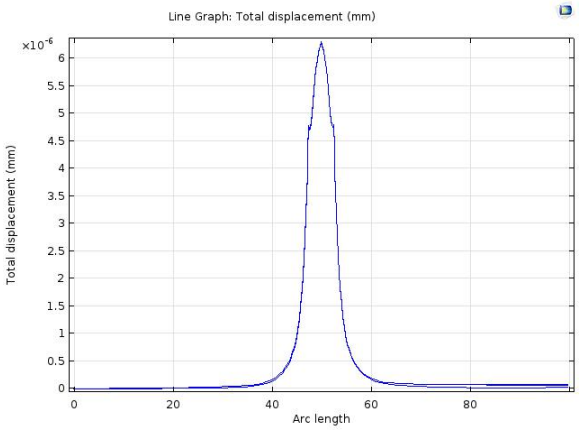

Figure 4. Plot of xz deformations at the top surface of the pipe when 20 volts are induced across the PZT patch

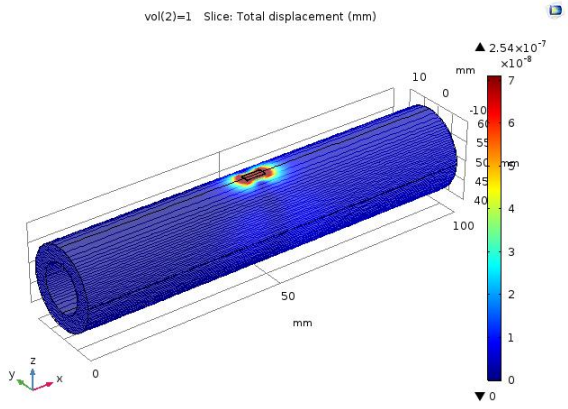

Figure 5. xy deformations when 1 V is induced across the PZT patch

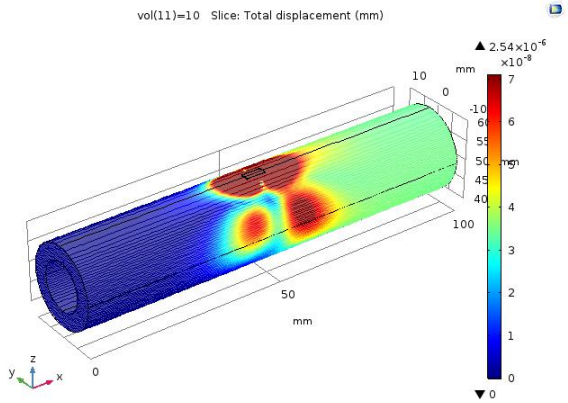

Figure 6. xy deformations when 10 volts are induced across the PZT patch

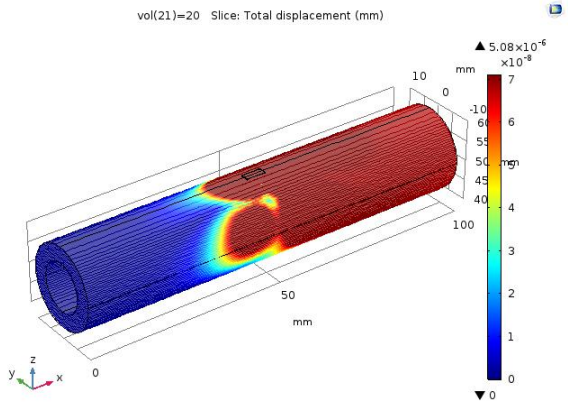

Figure 7. xy deformations when 20 volts are is induced across the PZT patch

The results show a gradual increase of the deformations until reaching a maximum magnitude at the center of the pipe at 50 mm from the left end, and a similar gradual decrease afterwards. This plot can help the pipeline engineers monitor the structural health of a pipe by approximating the deformation depth or location with respect to a fixed point. This method has a limited monitoring length as shown in the plot, which can be avoided by installing multiple sensors.

The next step is to study the deformations along the xy plane. This study aims at observing the horizontal deformations to relate the crack initiation to deformation propagation along the horizontal sections of the pipe. Figure 5 shows the pipe deformation when 1 volt is applied to the piezoelectric material. It shows that the deformation magnitudes are increasing in an outward circular motion towards the ends of the pipe. At this voltage, a maximum of 2.54 x 10^{-7} mm of deformation is observed. Figure 6 shows the pipe horizontal deformations when the voltage is increased to 10 volts. It shows that the deformations are increasing also, mainly towards the unconstrained side of the pipe. At this voltage, the maximum deformation is increased by one order of magnitude to 2.54 x 10^{-6} mm. Figure 7 shows the pipe horizontal deformations when the voltage is doubled to 20 volts. At this voltage, the maximum deformation is doubled too to a magnitude of 5.08 x 10^{-6} mm. Figures 5, 6, and 7 show a linear relationship between the maximum deformation observed at the pipe and the voltage induced through the PZT patch. These values can be used by the pipeline engineers as a baseline measurement to enhance structural health monitoring of the pipeline by detecting the horizontal location of anomalies with a better precision.

Finally, the deformations along the yz plane were simulated. Figure 8 shows yz cross sections of the total displacement along the pipeline when 20 volts are induced across the PZT patch. It shows a maximum deformation of 6.29 x 10^{-6} mm, similar to the value found from the xz plane. This similar value makes sense because the electric potential is induced from the surface along the xy plane, so the maximum deformations along the xz and yz should be similar. Figure 9 shows the yz cross section of the total displacement magnitudes along the pipeline when different electric potentials are induced across the PZT patch. This figure shows also the linear relationship between the electric potential and deformation magnitudes. In fact, at 1 volt electric potential, the maximum deformation is 3.14 x 10^{-7} mm, while at 10 volts, the deformation increased by 1 order of magnitude to 3.14 x 10^{-6} mm. In addition, when the voltage is doubled to 20 volts, the deformation is doubled too to 6.29 x 10^{-6} mm.

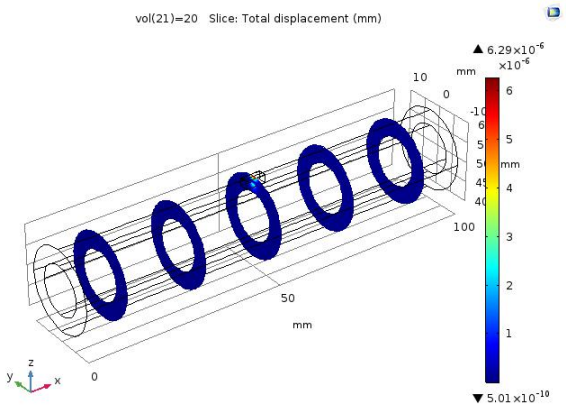

Figure 8. yz cross sections of the total displacement along the pipeline when 20 volts are induced across the PZT patch

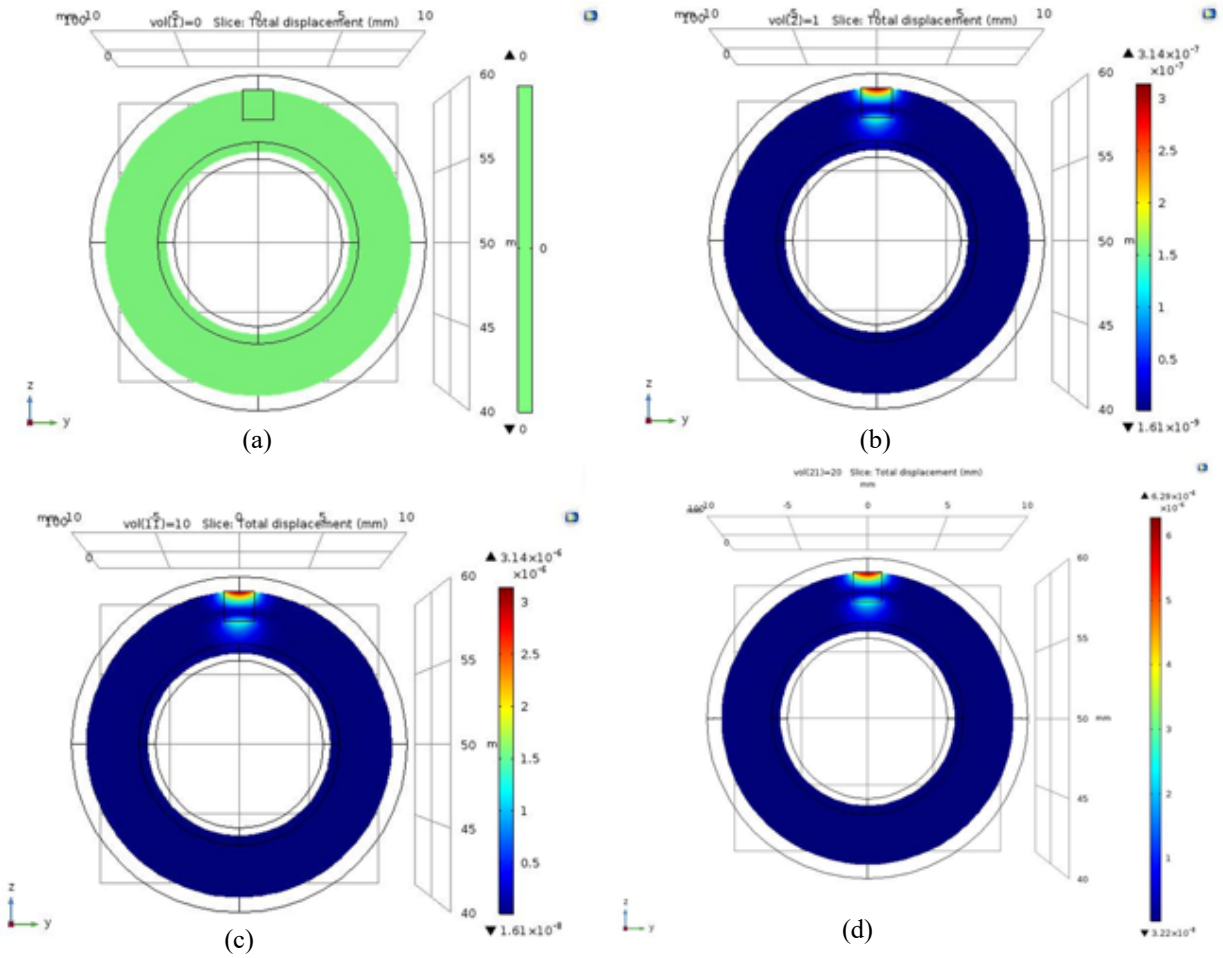

Figure 9. yz cross sections of the total displacement along the pipeline when different electric potentials are induced across the PZT patch: (a) 0 V, (b) 1 V, (c) 10 V, and (d) 20 V

The results presented in this section can be used by the pipeline engineers as a baseline measurement to detect anomalies, such as cracks or fractures in the pipe, and their magnitude by installing piezoelectric sensors along the pipeline. The continuous monitoring of the data provided by these sensors allows the detection of anomalies, and once a given voltage is read by the sensor, the results of this paper can be used to find the deformation magnitude, using interpolation or extrapolation if the exact voltage value does not match the exact baseline data.

Conclusions

This paper conducted a static and time-dependent analyses of a pipeline having an anomaly due to a piezoelectric actuator. An electric field is applied perpendicular to the poling direction, thereby introducing a transverse deflection or crack to the surface of the pipe. The results showed linear relationships between the induced voltage across the PZT patch and the magnitude of the deformations in the xy, xz, and yz directions. These results can act as baseline measurement to detect anomalies in pipelines based on continuously monitoring the piezoelectric sensor data with the obtained results.

Future work includes combining the results found in this paper with machine learning algorithms or statistical analysis methods to generate an algorithm to detect anomalies, their type and location with higher precision. In addition, future work includes adding another piezoelectric sensor at a predefined distance from the first one and induce high frequency waves between them to detect anomalies.

Acknowledgements

The authors would like to acknowledge the sponsorship of the Petroleum Institute, Khalifa University of Science and Technology, Abu Dhabi, UAE and the University of Maryland (Department of Mechanical Engineering) for the research work presented in this paper, which is part of the Pipeline System Integrity Management research project. In addition, the authors would like to acknowledge the SEAS-net Computing Facility and UCLA for proving the license to use COMSOL Multiphysics, which supported the numerical study.

References

[1] Chalgham, W., Seibi, A., and Lomas, M., 2016, "Leak Detection and Self Healing Pipelines Using Twin Balls Technology," *SPE Annual Technical Conference and Exhibition*, Society of Petroleum Engineers, SPE.

[2] Chalgham, W. R., Seibi, A. C., and Boukadi, F., 2016, "Simulation of Leak Noise Propagation and Detection Using COMSOL Multiphysics," *International Mechanical Engineering Congress and Exposition*, Phoenix, Arizona, USA.

[3] Chalgham, W. R., and Seibi, A. C., 2016, "Design of a Self-Recharging Untethered Mobile Inspection Tool inside a Pipeline," *COMSOL Multiphysics Conference*, Boston, MA.

[4] Chalgham, W. R., Seibi, A. C., and Mokhtari, M., 2016, "Simulation of Sound Wave Propagation Inside a Spherical Ball Submerged in a Pipeline," *COMSOL Multiphysics Conference*, Boston, MA.

[5] Seibi, A., and Chalgham, W., 2019, "Device and Method for Detecting Leaks and Healing Pipelines Using Twin Balls Technology."

[6] Chalgham, W. R., 2016, "Experimental and Numerical Investigation of Leak Detection in Pipelines," M.S., University of Louisiana at Lafayette.

[7] Karray, F., Garcia-Ortiz, A., Jmal, M. W., Obeid, A. M., and Abid, M., 2016, "EARNPIPE: A Testbed for Smart Water Pipeline Monitoring Using Wireless Sensor Network," Procedia Computer Science, **96**, pp. 285–294.

[8] Boaz, L., Kaijage, S., and Sinde, R., 2014, "An Overview of Pipeline Leak Detection and Location Systems," *Proceedings of the 2nd Pan African International Conference on Science, Computing and Telecommunications (PACT 2014)*, pp. 133–137.

[9] Muhlbauer, W. K., 2004, *Pipeline Risk Management Manual: Ideas, Techniques, and Resources*, Elsevier.

[10] Park, G., Cudney, H. H., and Inman, D. J., 2001, "Feasibility of Using Impedance-Based Damage Assessment for Pipeline Structures," Earthquake Engineering & Structural Dynamics, **30**(10), pp. 1463–1474.

[11] Choi, S., Song, B., Ha, R., and Cha, H., 2012, "Energy-Aware Pipeline Monitoring System Using Piezoelectric Sensor," IEEE Sensors Journal, **12**(6), pp. 1695–1702.

[12] Qing, X. P., Beard, S., Shen, S. B., Banerjee, S., Bradley, I., Salama, M. M., and Chang, F.-K., 2009, "Development of a Real-Time Active Pipeline Integrity Detection System," Smart Mater. Struct., **18**(11), p. 115010.

[13] Zhu, J., Ren, L., Ho, S.-C., Jia, Z., and Song, G., 2017, "Gas Pipeline Leakage Detection Based on PZT Sensors," Smart Mater. Struct., **26**(2), p. 025022.

[14] Sadeghioon, A. M., Metje, N., Chapman, D. N., and Anthony, C. J., 2014, "SmartPipes: Smart Wireless Sensor Networks for Leak Detection in Water Pipelines," Journal of Sensor and Actuator Networks, **3**(1), pp. 64–78.

Appendix

Table 1: Material Parameters of Pipeline

Description	Value
Density	2700[kg/m^3]
Electrical conductivity	{{35.5e6[S/m], 0, 0}, {0, 35.5e6[S/m], 0}, {0, 0, 35.5e6[S/m]}}
Coefficient of thermal expansion	{{23.1e-6[1/K], 0, 0}, {0, 23.1e-6[1/K], 0}, {0, 0, 23.1e-6[1/K]}}
Heat capacity	904[J/(kg*K)]
Thermal conductivity	{{237[W/(m*K)], 0, 0}, {0, 237[W/(m*K)], 0}, {0, 0, 237[W/(m*K)]}}
Young's modulus	70.0e9[Pa]
Poisson's ratio	0.35

Table 2: Material Parameters of the PZT Patch

Description	Value	Unit
Density	7500[kg/m^3]	kg/m³
Elasticity matrix (ordering: xx, yy, zz, yz, xz, xy)	{1.27205e+011[Pa],8.02122e+010[Pa], 1.27205e+011[Pa], 8.46702e+010[Pa], 8.46702e+010[Pa], 1.17436e+011[Pa], 0[Pa], 0[Pa], 0[Pa], 2.29885e+010[Pa], 0[Pa], 0[Pa], 0[Pa], 0[Pa], 2.29885e+010[Pa], 0[Pa], 0[Pa], 0[Pa], 0[Pa], 0[Pa], 2.34742e+010[Pa]}	Pa
Coupling matrix	{0[C/m^2], 0[C/m^2], -6.62281[C/m^2], 0[C/m^2], 0[C/m^2], -6.62281[C/m^2], 0[C/m^2], 0[C/m^2], 23.2403[C/m^2], 0[C/m^2], 17.0345[C/m^2], 0[C/m^2], 17.0345[C/m^2], 0[C/m^2], 0[C/m^2], 0[C/m^2], 0[C/m^2], 0[C/m^2]}	C/m²
Relative permittivity	{1704.4, 1704.4, 1433.6}	1

Table 3: Strain-charge form Settings of the PZT Patch

Description	Value
Compliance matrix (ordering: xx, yy, zz, yz, xz, xy)	{{1.65e-011[1/Pa], -4.78e-012[1/Pa], -8.45e-012[1/Pa], 0[1/Pa], 0[1/Pa], 0[1/Pa]}, {-4.78e-012[1/Pa], 1.65e-011[1/Pa], -8.45e-012[1/Pa], 0[1/Pa], 0[1/Pa], 0[1/Pa]}, {-8.45e-012[1/Pa], -8.45e-012[1/Pa], 2.07e-011[1/Pa], 0[1/Pa], 0[1/Pa], 0[1/Pa]}, {0[1/Pa], 0[1/Pa], 0[1/Pa], 4.35e-011[1/Pa], 0[1/Pa], 0[1/Pa]}, {0[1/Pa], 0[1/Pa], 0[1/Pa], 0[1/Pa], 4.35e-011[1/Pa], 0[1/Pa]}, {0[1/Pa], 0[1/Pa], 0[1/Pa], 0[1/Pa], 0[1/Pa], 4.26e-011[1/Pa]}}
Coupling matrix (ordering: xx, yy, zz, yz, xz, xy)	{{0[C/N], 0[C/N], -2.74e-010[C/N], 0[C/N], 0[C/N], -2.74e-010[C/N]}, {0[C/N], 0[C/N], 5.93e-010[C/N], 0[C/N], 7.41e-010[C/N], 0[C/N]}, {7.41e-010[C/N], 0[C/N], 0[C/N], 0[C/N], 0[C/N], 0[C/N]}}
Relative permittivity	{{3130, 0, 0}, {0, 3130, 0}, {0, 0, 3400}}
Loss factor for compliance matrix sE	{{0, 0, 0, 0, 0, 0}, {0, 0, 0, 0, 0, 0}, {0, 0, 0, 0, 0, 0}, {0, 0, 0, 0, 0, 0}, {0, 0, 0, 0, 0, 0}, {0, 0, 0, 0, 0, 0}}
Loss factor for coupling matrix d	{{0, 0, 0, 0, 0, 0}, {0, 0, 0, 0, 0, 0}, {0, 0, 0, 0, 0, 0}}
Loss factor for electrical permittivity εT	{{0, 0, 0}, {0, 0, 0}, {0, 0, 0}}

Table 4: Stress-charge form Settings of the PZT Patch

Description	Value
Elasticity matrix (ordering: xx, yy, zz, yz, xz, xy)	{{1.27205e+011[Pa], 8.02122e+010[Pa], 8.46702e+010[Pa], 0[Pa], 0[Pa], 0[Pa]}, {8.02122e+010[Pa], 1.27205e+011[Pa], 8.46702e+010[Pa], 0[Pa], 0[Pa], 0[Pa]}, {8.46702e+010[Pa], 8.46702e+010[Pa], 1.17436e+011[Pa], 0[Pa], 0[Pa], 0[Pa]}, {0[Pa], 0[Pa], 0[Pa], 2.29885e+010[Pa], 0[Pa], 0[Pa]}, {0[Pa], 0[Pa], 0[Pa], 0[Pa], 2.29885e+010[Pa], 0[Pa]}, {0[Pa], 0[Pa], 0[Pa], 0[Pa], 0[Pa], 2.34742e+010[Pa]}}
Coupling matrix	{{0[C/m^2], 0[C/m^2], -6.62281[C/m^2], 0[C/m^2], 0[C/m^2], -6.62281[C/m^2]}, {0[C/m^2], 0[C/m^2], 23.2403[C/m^2], 0[C/m^2], 17.0345[C/m^2], 0[C/m^2]}, {17.0345[C/m^2], 0[C/m^2], 0[C/m^2], 0[C/m^2], 0[C/m^2], 0[C/m^2]}}
Relative permittivity	{{1704.4, 0, 0}, {0, 1704.4, 0}, {0, 0, 1433.6}}
Loss factor for elasticity matrix cE	{{0, 0, 0, 0, 0, 0}, {0, 0, 0, 0, 0, 0}, {0, 0, 0, 0, 0, 0}, {0, 0, 0, 0, 0, 0}, {0, 0, 0, 0, 0, 0}, {0, 0, 0, 0, 0, 0}}
Loss factor for coupling matrix e	{{0, 0, 0, 0, 0, 0}, {0, 0, 0, 0, 0, 0}, {0, 0, 0, 0, 0, 0}}
Loss factor for electrical permittivity εT	{{0, 0, 0}, {0, 0, 0}, {0, 0, 0}}

Table 5: Material parameters of Water

Description	Value
Dynamic viscosity	eta(T[1/K])[Pa*s]
Ratio of specific heats	1.0
Electrical conductivity	{{5.5e-6[S/m], 0, 0}, {0, 5.5e-6[S/m], 0}, {0, 0, 5.5e-6[S/m]}}
Heat capacity at constant	Cp(T[1/K])[J/(kg*K)]
Density	rho(T[1/K])[kg/m^3]
Thermal conductivity	{{k(T[1/K])[W/(m*K)], 0, 0}, {0, k(T[1/K])[W/(m*K)], 0}, {0, 0, k(T[1/K])[W/(m*K)]}}
Speed of sound	cs(T[1/K])[m/s]

Table 6: Mesh Properties

Description	Value
Maximum element size	5.5
Minimum element size	0.4
Curvature factor	0.4
Resolution of narrow regions	0.7
Maximum element growth rate	1.4
Predefined size	Finer
Minimum element quality	6.747E-5